

Full Length Article

Oxidative vaporization etching for molybdenum tip formation in air

Yuto Goto^a, Rie Suizu^b, Yutaka Noguchi^c, Toyo Kazu Yamada^{a,d,*}^a Department of Materials Science, Chiba University, 1-33 Yayoi-cho, Inage-ku, Chiba 263-8522, Japan^b Department of Chemistry, Nagoya University, Furo-cho, Chikusa-ku, Nagoya 464-8602, Japan^c School of Science and Technology, Meiji University, Kanagawa 214-8571, Japan^d Molecular Chirality Research Centre, Chiba University, 1-33 Yayoi-cho, Inage-ku, Chiba 263-8522, Japan

ARTICLE INFO

Keywords:

Molybdenum
Tip probe
Oxidative vaporization
Molybdenum oxides
Scanning tunneling microscopy
Conductance

ABSTRACT

Oxidative vaporization in air using a flame with a temperature range of 1950–2300 K was employed for controlling the tip shape made from a nipper-cut metal molybdenum (Mo) wire edge. An extremely high vapor pressure of MoO₃ generated on the Mo surface in flame is a driving force behind the tip shape formation. Since the MoO₃ vaporization rate follows the flame temperature gradient, we could control the tip apex shape by selecting the proper flame etching condition. The best condition to obtain a sharp tip apex based on statistical tests of dozens of Mo tips was obtained by Mo wire edge insertion into the 2100 K flame from the side for one second. This was repeated twice, which reproducibly provided a tip apex with a radius of 50–100 nm and a cone angle of 20–30 degrees. The present Mo tips, fabricated without aqueous solutions, were examined for their suitability as probe tips through air-scanning tunneling microscopy (STM), ultrahigh vacuum STM, field emission spectroscopy, and conductance measurements.

1. Introduction

Numerous techniques for producing metallic nano tip probes have been widely developed in recent decades [1–19], ever since the precise detection of electrons, holes, and ions through a single atom / molecule or nano dot has provided a deeper insight into the charge transfer mechanism [20,21], direct visualizations of sample surface states [22,23], molecular orbital states [24,25], and quantum spin states [26,27]. Consequently, this has offered tremendously diverse possibilities for the development of atomic-size devices in single molecular electronics [28–30], single atom / molecule spintronics [21,31–33], topological electronics [34,35], and high-frequency devices [36,37].

Nowadays metallic tip probes support a wide variety of nanoscience research fields, which are often used as four- or two-point probes for surface conductance measurements [38,39] or nano-wire resistance measurements [40–42]. Sharp metallic tips have also been used in field ion microscopy [43,44], field emission scanning electron microscopy (FE-SEM) [45,46], scanning tunneling microscopy (STM) [47], and q-plus sensor atomic force microscopy [48].

The most commonly used tungsten (W) or noble metal platinum-iridium (PtIr) probe tips have been fabricated via aqueous chemical etching treatments [2–6,15–19,44,46]. Alongside these aqueous

chemical etching methods, a further innovative method without aqueous solutions for constructing tip probes from metal wire have also been developed, which employed a drastic change of the vapor pressure between metal and its oxides. For example, tungsten has a very low pressure of 10⁻⁸ Torr at 2400 K (higher than the flame temperature), but the vapor pressure drastically increases when the W changes to WO₃; e.g. 760 Torr at 1900 K. Using this oxidative vaporization property with the temperature gradient in the flame, a sharp W tip probe was produced within a few seconds in air, by simply using a liquefied petroleum (LP) and oxygen (O₂) gas flame [1].

However, this oxidative vaporization etching was not suitable for noble metals. Since their melting temperatures are lower than a highest flame temperature of 2300 K, the noble metal wire edge formed a ball shape instead of a tip shape. On the other hand, W and Mo have a melting temperature of 3695 K and 2890 K, respectively, which are much higher than the flame temperature. Therefore, they should not be melted by the flame. Markedly, with our eyes, the W wire edge was confirmed to be changed to a clear tip shape via the oxidative vaporization. However, the Mo wire edge formed a ball shape. This is unusual since Mo should not be melted and almost no vaporization at the flame temperature.

Hence, the present study focuses to unveil the oxidation process at

* Corresponding author at: Department of Materials Science, Chiba University, 1-33 Yayoi-cho, Inage-ku, Chiba 263-8522, Japan.

E-mail address: toyoyamada@faculty.chiba-u.jp (T.K. Yamada).

the Mo wire edge inside the flame, and we will show that a sharp Mo tip shape formation can be provided by tuning the MoO_3 vaporization rate.

2. Methods

2.1. Flame etching

Fig. 1a shows the flame setup. Herein, a typical mixture of liquefied petroleum (LP) and oxygen gas was used. We used a commercial micro torch (an aperture with a diameter of 0.5 mm) to obtain a reproducible flame of constant size, with the same temperature. The flame consists of

two regions: an inner oxygen-poor white flame and an outer oxygen-rich blue flame. The flame temperature was measured using an Ir-IrRh40 thermocouple (Furuya Metal Co., Ltd.). $x = 0$ mm is defined as the centre of the flame, and $y = 0$ mm is defined as the top of the micro torch from which the flame is emanating (see Fig. 1a). The flame temperature along the flame axis ($x = 0$, $y = 0$ –42 mm) denoted a highest temperature of 2300 K at $y = 5$ mm, at the boundary between the inner and the outer flame. The temperature gradually decreased to 2100 K at $y = 15$ mm. Subsequently, at a value greater than $y = 30$ mm, the temperature dropped below 1700 K (see Supplementary Material, Fig. S1). We also checked the flame temperature perpendicular to the flame axis (along

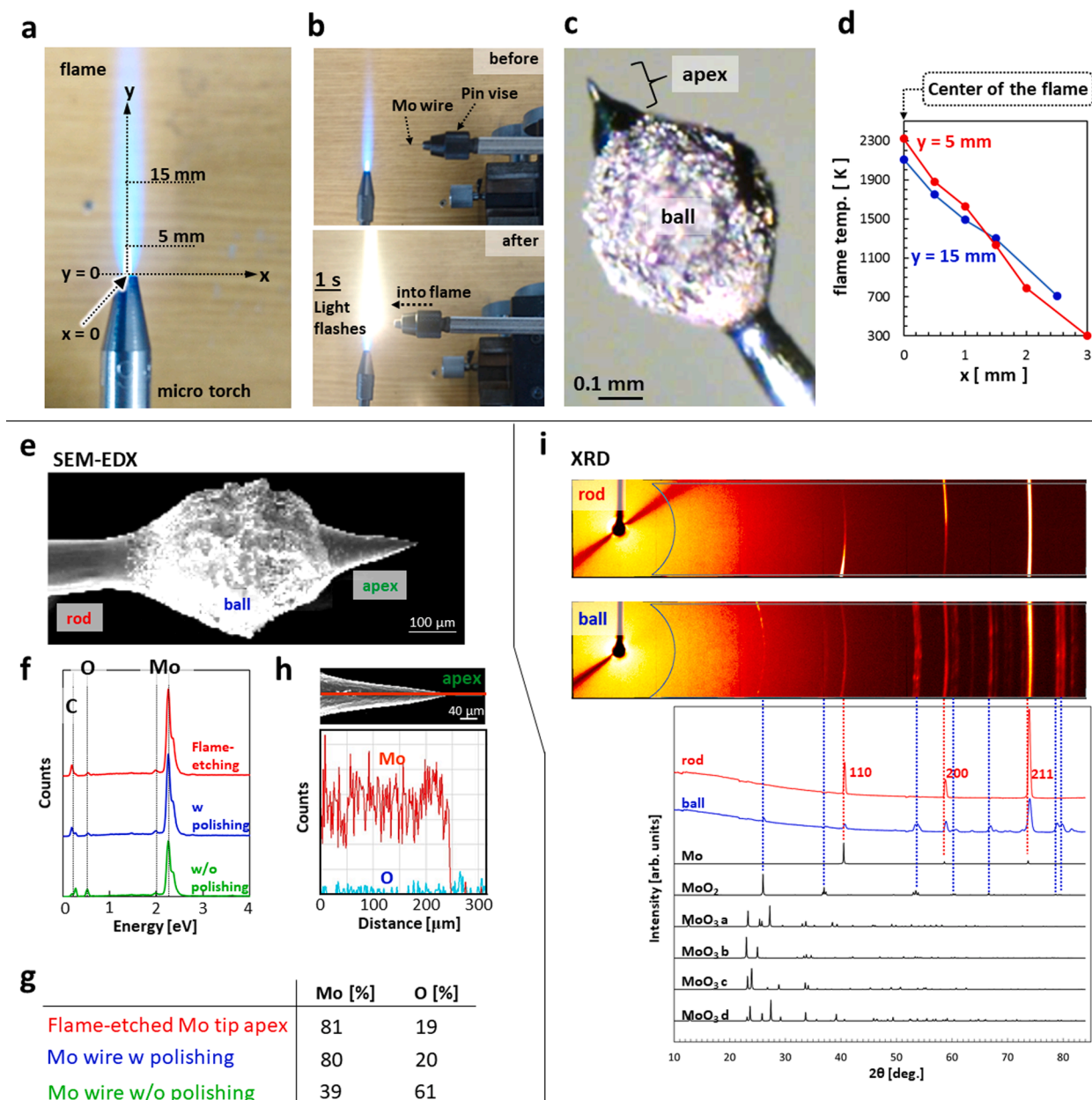


Fig. 1. (a) Gas flame with x and y axes. (b) Before and after the Mo wire edge placed in the flame. (c) Optical microscopy image of the Mo wire edge after the flame insertion. (d) Flame temperatures as a function of the x -axis. Red and blue lines denote flame temperatures measured at $y = 5$ and 15 mm, respectively. (e–h) SEM-EDX chemical identification of the flame-etched Mo tips. (e) SEM image of apex, ball and rod regions. (f) SEM-EDX results obtained from the apex region after flame etching (red), a Mo wire surface with polishing (blue), and a Mo wire surface without polishing (green). (g) Composite material percentages obtained from SEM-EDX peaks obtained from the apex region after flame etching (red), a Mo wire surface with polishing (blue), and a Mo wire surface without polishing (green). (h) SEM-EDX one-dimensional mapping along the line in the SEM image. (i) X-ray diffraction results obtained from the ball and the rod regions. X-ray diffraction intensity plot as a function of 2θ obtained from the rod (red line) and ball (blue line) regions. Black lines denote reference plots of Mo, MoO_2 , MoO_3 type-a, MoO_3 type-b, MoO_3 type-c, and MoO_3 type-d. Experimentally obtained peaks are identified as Mo and MoO_2 . Melted MoO_2 forms the ball-shape region.

the x-axis) as depicted in Fig. 1d, since the Mo wire was inserted into the flame from the side in this study. Along this axis, a highest temperature of 2300 K ($y = 5$ mm) and 2100 K ($y = 15$ mm) was measured at the center of the flame ($x = 0$ mm). The temperature then decreased linearly and dropped below 1400 K at $x = 1.5$ mm.

A Mo wire (diameter $\varphi = 0.20$ mm, purity 99.95%) was cut off by a nipper with a length of 10–15 mm and fixed by a metal wire holder (so-called pin vise, see Fig. 1b). The wire edge was then inserted perpendicular to the flame axis from the side. We used a linear course motion stage, which ensured good reproducibility of forward and backward insertion of the wire edge into the flame. We used a constant insertion time period of approximately 1 s, corresponding to one etching cycle. During these cycles, we consistently observed light flashes (see Fig. 1b, lower panel). After the flashes, the Mo wire edge always formed a ~ 0.5 mm size ball. However, we found that an apex region was also formed on the ball (see Fig. 1c).

2.2. SEM, EDX and X-ray diffraction measurements

A compact Tiny-SEM (Technex Lab. Co. Ltd., operation pressure 10^{-2} Pa, electron beam energy 10 keV) was used to verify the shape of the Mo wire edge before and after the flame etching. SEM images were obtained within 30 min of the flame etching. Chemical identification of the flame etched Mo tips was performed with X-ray diffraction (XRD) and SEM energy dispersive X-ray (EDX) spectroscopy. X-ray data were recorded with the Bruker AXS Smart APEX Ultra by using graphite-monochromated $\text{CuK}\alpha$ radiation ($\lambda = 1.54178$ Å). The SEM JSM-6510A (JEOL) was used for EDX measurements.

2.3. UHV-STM measurements

A home-built ultrahigh vacuum (UHV) STM setup operated at 300 K was used. The setup included introduction, preparation, and analytical chambers (base pressure: 10^{-8} Pa). The gate valves separated each chamber; therefore, we could transfer the tip and an Au(001) sample through the introduction chamber without breaking the vacuum of other two chambers. The tip was flushed to 2300 K (emission current 60–80 mA with acceleration bias 0.5 kV) inside the preparation chamber to reduce the Mo-oxide film thickness [44]. A clean and atomically-flat Au (001) surface was obtained by repeating Ar^+ sputtering (750 eV) and annealing (743 K) cycles in the preparation chamber. The cleaned tip and sample were transferred to the analytical chamber and set into the STM. STM and scanning tunneling spectroscopy (STS) measurements were carried out by combining the Nanonis BP4 SPM controller and the corresponding software. The topographic images were obtained in a constant current mode. STS was carried out by measuring tunneling current as a function of the sample bias voltage ($I(V)$ curve) at each pixel position in an STM topographic image (feedback off). Background-excluding treatments of the original STM topographic images, and the process of extracting the $I(V)$ curves from the original data, were performed with the WSxM 5.0 Develop 9.1 software [62].

2.4. Air-STM measurements

A commercial STM setup was used in air (JEOL 4200) [63,64]. Highly oriented pyrolytic graphite (HOPG) was cleaved by using a scotch tape in air and then set inside the STM stage. The flame-etched Mo tip was approached on the cleaved surface and STM measurements were performed in a constant current mode using the JEOL software. $I(V)$ curves were measured under feedback off. The WSxM 5.0 Develop 9.1 software was used for data analysis [62].

2.5. Field emission curve measurements

A home-built UHV field emission (FE) setup was used [44]. The flame-etched Mo tip was set in the tip stage. A counter electrode (W

filament) was then placed in front of the Mo tip apex (2 mm separation). A negative bias voltage was applied to the tip side, and emission current from the tip apex was simultaneously measured by the counter electrode. An exponentially increased FE curve was obtained above the threshold bias voltage. Our setup measured the current up to 50 nA and immediately stopped the application of the bias via a Lab View control.

2.6. Tip probe conductance measurements

A commercial vacuum probe station was used (Riko International Ltd. i-series). The measurement setup is shown in Fig. 4a. The test sample was an evaporated gold film prepared by the template stripping method [52]. The thickness of the gold film was ~ 500 nm. Two probes contacted on the gold surface, where one was a standard W probe while the other was the flame-etched Mo probe. As a reference, a nipper-cut Mo wire and standard W probe were also used as the second probe. The current–voltage curves were measured in air using a source measure unit (Keithley 2636A).

3. Results and discussion

Fig. 1e shows a SEM image of the flame etched Mo tip in the vicinity of the apex. We divided this area into three distinct regions: apex, ball, and rod. The apex region has a smooth surface, and grains or grain boundaries are not observed. The ball region includes many grains. The rod region has a smooth surface and no grain formation is observed. SEM-EDX measurements were performed for the apex, ball, and rod regions by focusing the electron beam on each region. All regions showed peaks at the same energy levels, and it was found that there were three chemicals on the surface, namely Mo, oxygen (O), and carbon (C) (see Fig. 1f). The presence of the carbon peaks in most likely explained by the fact that we used a carbon tape as a background substrate. EDX quantitative analysis results are summarized in the table in Fig. 1g. We found that the apex surface of the flame-etched Mo tip consists of Mo: 81% and O: 19%. Meanwhile, one might note that the EDX results indicate oxidization at the apex. This oxidization could be occurred during the LP + O_2 flame etching or natural oxidization in air after the flame treatment. In order to understand how the flame etching contributes to the oxidization, we compared EDX measurements for the Mo apex before and after the flame etching. The results were shown in the table in Fig. 1g. Before the flame etching, the Mo apex surface consists of Mo: 39% and O: 61%, namely the Mo surface in air is coated by a thick oxide film. However, after the flame etching, a drastic decrease of the oxidization occurred: Mo: 81% and O: 19%. As a reference, we also polished the Mo wire surface and removed the thick oxide film. Then the polished Mo showed Mo: 80% and O: 20%, which is comparable to the flame-etched Mo tip apex. These prove that the flame etching does not enhance the oxidization, but excludes the thick oxide film. The remained oxygen peak in the EDX measurement could be due to oxidization in air after the flame etching. One-dimensional EDX mapping was also performed on the Mo tip apex region (see Fig. 1h), which clearly revealed that the Mo is the majority element at the apex.

Further chemical identification of the flame etched Mo tip was performed using X-ray diffraction (XRD). Fig. 1i shows XRD data obtained at the ball and rod regions. By comparing this data with the reference data of Mo metal and Mo-oxides (MoO_2 and four polymorphs of MoO_3 , see Supplementary Material, Fig. S5), the experimentally obtained XRD peaks at the ball and rod can be identified as MoO_2 and Mo, respectively. We further obtained Laue spots at the apex, ball, and rod regions (see Supplementary Material, Fig. S4), indicating that neither the apex nor the ball regions consist of a single domain, but rather each includes several larger differently oriented domains. However, the rod region did not exhibit any orientation (polycrystal).

The XRD and SEM-EDX results in Fig. 1e-i identify that the generated ball consists of MoO_2 , while the tip apex consists of Mo. No MoO_3 was remained. These experimental evidences are well explained by the Mo-

oxide phase transition process [49–51,53,54]. Mo first becomes MoO_3 at 673 K, and then changes to MoO_2 above 700 K. Interestingly, MoO_2 has a lower vapor pressure (10^{-4} atmosphere (atm) at 1818 K) with a melting point of 1373 K, which is the cause of the MoO_2 ball generation at the lower flame temperature region. On the other hand, MoO_3 has extremely high vapor pressures: e.g. 10^{-3} atm at 1000 K, 0.5 atm at 1350 K, and 1 atm at 1424 K, namely the generated MoO_3 inside the flame was immediately vaporized, and therefore there is no MoO_3 after the Mo flame etching as confirmed by the XRD measurements in Fig. 1i. Because of the linear temperature gradient inside the flame along the x axis (see Fig. 1d), the center of the flame has the highest MoO_3 vaporization rate, thus providing the tip shape.

Now we focus on the fabrication process of the apex region. Fig. 2a show SEM images obtained from the Mo wire edges after the flame insertion using different temperatures: from left to right, 1450, 1850, 1950, 2100, 2250 and 2300 K. Although MoO_3 was generated above 673 K and the vapor pressure increases to 1 atm at 1424 K according to the phase diagram [49–51,53,54], the MoO_3 vaporization rate is not

enough to produce a tip shape for 1450–1850 K. We could still see the original nipper-cut edge shape. However, starting from 1950 K to 2300 K, the apex showed a clear tip shape. It is noted that the cone angle of the apex changed at different temperatures. The 2100–2250 K flame produced a sharper cone angle, but the 2300 K flame produced a blunter apex, indicating too high MoO_3 vaporization rate could render the apex blunter.

Fig. 2b shows models of generation and vaporization of MoO_3 inside the flame. As shown in Fig. 2a, depending on different temperature flames, regular to irregular shape morphology was produced at the apex. Because of the insertion position into the flame, we could choose different temperature gradient inside the flame (see Fig. 1d), and this temperature gradient controls the apex morphology. Three models in Fig. 2b represent how different temperature gradients change the morphology using larger MoO_3 vaporization rate at higher temperature. Color bars indicate the flame temperature. The size of the black circles denotes a vaporization rate of MoO_3 at each position, which is determined by local temperature. Using the flame with a temperature range

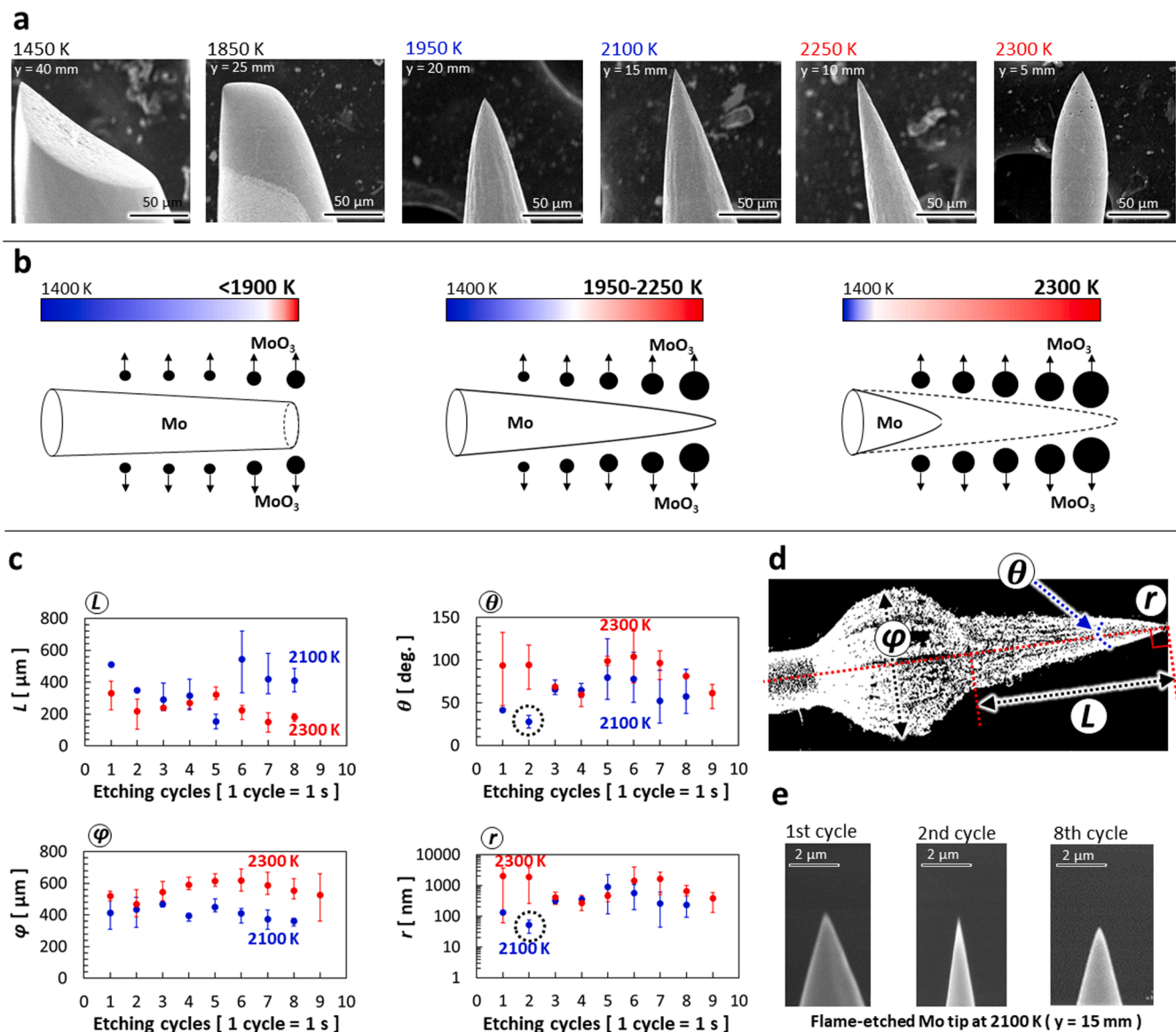


Fig. 2. (a) SEM images of Mo tip apices flame-etched at 2300 K, 2250 K, 2100 K, 1950 K, 1850 K, and 1450 K. (b) Models of MoO_3 vaporization etching at different flame temperatures. Left panel: 1400–1900 K, center panel: 1400–2250 K, and right panel: 1400–2300 K. (c) Statistical data obtained from hundreds of SEM images for dozens of flame-etched Mo tips, representing a dependence of L , ϕ , θ , and r on the flame-etching cycles. Mo tips etched at $y = 5$ mm (2300 K, red dots) and $y = 15$ mm (2100 K, blue dots) were used. (d) SEM image of the flame-etched Mo tip. Apex length (L), ball diameter (ϕ), cone angle (θ), and tip radius (r) are defined. (e) SEM images of the Mo tip apices after the flame etching cycles of 1, 2, and 8 times.

of 1400–1900 K (left model), the MoO_3 vaporization rate is low and no big difference between the rod and the apex regions, hence the Mo wire becomes narrow, but no tip shape was formed.

However, when we use the flame with a temperature range of 1400–2250 K (see center model in Fig. 2b), the MoO_3 vaporization rate at the apex is suitably higher than the rod region, a tip-shape

morphology is formed, while if one uses the 1400–2300 K flame, the vaporization rate at the apex region becomes too high, hence rendering the tip apex blunter (see right model in Fig. 2b).

During the flame etching, we found that the Mo atoms in the apex region moved even the flame temperature was much lower than the melting temperature of 2890 K since X-ray Laue spots appeared after the

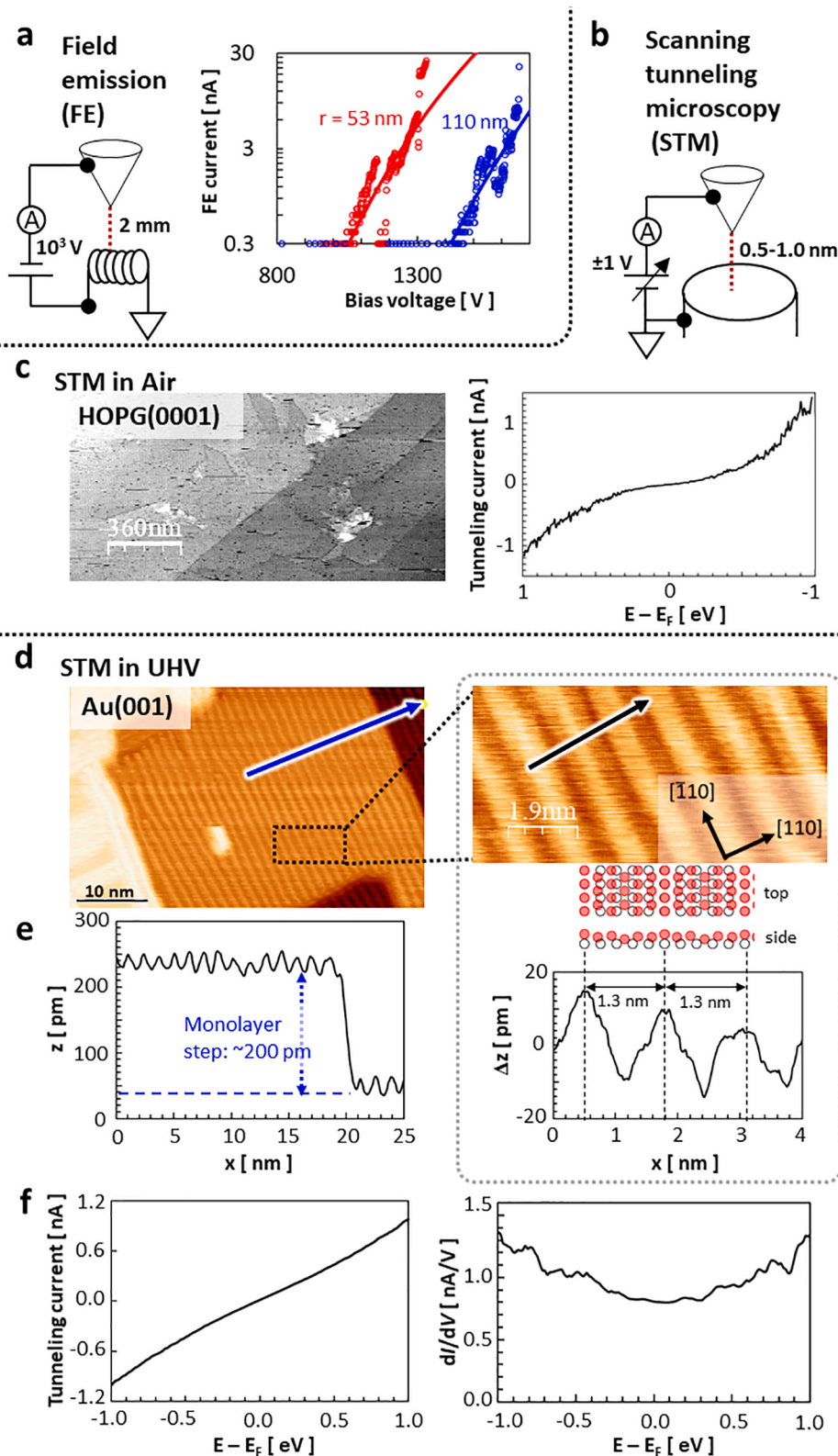


Fig. 3. Testing the flame-etched Mo tip probes. (a) Field emission (FE) spectroscopy measurements. FE curves were obtained after 5 (blue dot) and 11 (red dots) flushing treatment in UHV. Fitted Fowler-Nordheim plots show the tip radii of 110 and 53 nm. (b) Scanning tunneling microscopy (STM) model. (c) STM topographic image obtained on a cleaved HOPG(0001) surface in air (1890 × 910 nm², V_s = -1 V, I_t = 500 pA). The right panel denotes an I(V) curve obtained on the HOPG(0001) (setpoint V_s = -1 V, I_t = 1 nA). E_F denotes the Fermi energy. (d) STM topographic image obtained on a cleaned Au(001) surface at 300 K in UHV (50 × 30 nm², V_s = -1 V, I_t = 1 nA), and the enlarged image (right panel, 9.5 × 4.8 nm², V_s = -100 mV, I_t = 1 nA). (e) Height profile along the arrow in (d). (f) I(V) and dI/dV curve obtained on the Au(001) (setpoint V_s = -1 V, I_t = 1 nA). E_F denotes the Fermi energy.

flame etching (see [Supplementary Information](#)). When MoO₃ was formed and immediately vaporized, fresh Mo atoms appeared. These Mo atoms were immediately changed to MoO₃ because of the presence of oxygen in the flame, and vaporized again. This process was repeated. Simultaneously, the Mo atoms could diffuse on the surface and form a flat and smooth surface at the apex.

Thus, proper MoO₃ vaporization etching rate is required to obtain a sharp tip formation. We systematically flame-etched and carefully analysed the tip apexes using SEM to find the best conditions to provide a sharper tip shape formation with a good reproducibility. [Fig. 2c](#) shows the statistical results obtained based on dozens of the flame etched Mo tips from hundreds of SEM images (some examples are shown in [Supplementary Material, Figs. S2 and S3](#)).

To perform the statistical measurements, it was necessary to define the flame etching process in further detail. We used the course motion to reproduce the same flame etching condition ([Fig. 1b](#)). We placed the Mo wire edge into the flame from the side, and waited 1 s during the flashing, then pulled the Mo wire from the flame. This 1 s flashing motion was defined in this study as one etching cycle. We repeated this process 1–10 times. At each cycle, the tip shape was monitored using SEM. Based on the hundreds of the SEM images obtained, we quantitatively characterized four parameters as depicted in [Fig. 2d](#): a length of the tip formation region (L), a diameter of the ball region (φ), a cone angle of the apex (θ), and a tip radius (r). The tip radius r is the radius of the local curvature at the forefront tip apex, which was obtained by a parabolic curve fit: $y = ax^2 + bx + c$ and $r = (2a)^{-1}$. [Fig. 2c](#) shows a summary of the data obtained at a flame position of $y = 5$ mm (red dots, 2300 K) and $y = 15$ mm (blue dots, 2100 K).

The length of the tip apex region (L) varied between 100 and 600 μm (see [Fig. 2c](#)), but it seems that etching with a 2100 K flame produced a larger tip apex length. This is a good agreement with the models in [Fig. 2b](#), namely the 2300 K etching was too powerful and made the apex length shorter. This also relates to the cone angle (θ) and the tip radius (r), i.e., the 2100 K etching provides sharper tips. Further, the MoO₂ ball diameter was approximately 400 μm for 2100 K and approximately 600 μm for 2300 K, indicating the higher temperature encouraged more Mo changes to MoO₂. Repetition of the flame etching did not produce significant changes of the ball size.

[Fig. 2e](#) shows SEM images obtained from the Mo tip apex after 1, 2 and 8 cycles of the 2100 K etching. The cone angle is drastically changed by the numbers of the cycles. Therefore, the number of etching cycles is also important factor to get a sharp apex.

Through these statistical measurements in [Fig. 2c](#), the 2100 K flame etching was better to produce a sharper tip rather a highest temperature of 2300 K. So far we found that the best condition to reproducibly produce an apex with a cone angle of $\theta = 20$ –30 degrees and a radius of $r = 50$ –100 nm was a Mo wire edge insertion into the 2100 K flame ($y = 15$ mm) for 1 s repeating twice (see [Fig. 2c](#), marked by a dotted circle).

Chemically etched Mo tip probes have been used as a scanning probe tip, a field emission cathode tip, and a sample holder in nano-scientific research [55–57]. Here, we show that the oxidative vaporized Mo tips also provided the same quality. Firstly, a field emission test in UHV was carried out (see [Fig. 3a](#)) [44]. The flame etched Mo tip in air was introduced into the UHV field emission (FE) tip stage; subsequently, negative bias was applied to the Mo tip (0–3000 V, producing a 0–10⁶ V/m electric field). No field emission was produced, suggesting that the flame-etched Mo tip apex could be covered by an oxide film or be contaminated. This is normal since the flame etching process was done in air. However, after five flushing cycles in UHV (2300 K) using electron bombardment, we successfully measured a field emission current shown as red dots in [Fig. 3a](#). Since this is similar to the chemically etched W tip case [44], the flame-etched Mo tip apex could be coated by an oxide thin film due to oxygen absorption in air as pointed by the SEM-EDX measurements in [Fig. 1g](#). The radii of the flame-etched Mo tips were obtained with a fit of Fowler-Nordheim plot based on a semi-spherical apex model (solid lines in [Fig. 3a](#)). The experimentally obtained field

emission (I) curves as a function of the applied bias (V) to the tip was fitted by $I = (2\pi^2) \times 1.537 F^2 \times 10^{14} / (\Phi t^2(y)) \exp(-0.683 \Phi^{1.5} \omega(y) / F)$, where F denotes the electric field at the apex: $F = 0.368 V / (r^{0.9} (d^{0.1} - 0.75 r^{0.1}))$, $y = 3.79 F^{1/2} / \Phi$, $t(y) = 0.9967 + 0.0716 y + 0.0444 y^2$, $\omega(y) = 1.0029 - 0.1177 y + 1.1396 y^2 - 0.2561 y^3$, tip-anode distance (d): 0.002 m, work function of Mo(1 1 0) (Φ): 4.95 eV [8,44]. The tip radius was evaluated as $r = 110$ nm. We further repeated the UHV flushing. The blue dots were obtained after 11 flushing cycles with a radius of $r = 53$ nm, indicating a further reduction of the Mo-oxide film thickness. The range of radii for flame-etched Mo tips was thus shown to be 50–100 nm.

Secondly, the flame-etched Mo tip was tested as an air-STM probe tip (see [Fig. 3b](#)). A flame etched Mo tip was set in the air-STM setup and approached on the cleaved HOPG surface. Although we expected a crash of the flame-etched Mo tip because of the oxide film coating on the Mo tip apex, the Mo tip detected the tunneling current and safely stopped the approach without a tip crash in air. The obtained STM topographic image is shown in [Fig. 3c](#). Atomic terraces and monolayer steps are observed, but scratch-like noises are also observed. The $I(V)$ curve obtained on the same surface showed no band gap around the Fermi energy and displayed an exponential increase for both the negative and positive bias sides, indicating the metallic property of the flame etched Mo tip in air. One might deduce that the scratch-like noises included in the topographic image and the $I(V)$ curve could be due to the remaining Mo-oxide coating the apex.

Thirdly, the flame etched Mo tip produced in air was tested as a UHV-STM probe tip [58–61]. Here, the Mo tip was flushed to clean the apex in the UHV preparation chamber. [Fig. 3d](#) shows an STM topographic image obtained on a clean Au(001) surface with the flame etched Mo tip. Surface reconstructed (5×20) or (5×28) stripe patterns along the $\langle 110 \rangle$ direction are clearly observed on the atomic terraces [65]. A height profile along the blue arrow in [Fig. 3d](#) is shown in [Fig. 3e](#), where a fcc-Au(001) monolayer step height of ~ 200 pm is confirmed. An enlarged STM image obtained on the terrace emphasized the surface reconstruction. The height profile along the black arrow indicates a stripe with a 1.3 nm periodicity (20 pm height corrugation). Sphere models denote top and side views of the Au(001) surface reconstruction, where red and white ball correspond to surface and sub-surface atoms, respectively. $I(V)$ and dI/dV curves obtained on the Au(001) surface showed no gap ($dI/dV \neq 0$ at the Fermi energy), but did show an exponential increase for both the negative and positive bias sides, indicating that the Mo tip has metallic properties (see [Fig. 3f](#)). Comparing the results in [Fig. 3f](#) with the ones in [Fig. 3c](#), the scratch-like noise decreased drastically, indicating that UHV flushing is a promising treatment for reducing the Mo-oxide adsorbed on the apex. Since these testing results showed a comparable quality with the STM results obtained by using a chemically etched Mo tip [55], the flame-etched Mo tip could be also used as an STM probe tip.

Finally, we examined the flame-etched Mo tips as a probe for a two-point contact conductance measurement. [Fig. 4a](#) show the setup. One electrode was used as a standard W tip probe. As the other electrode, we examined several tip probes, namely two flame-etched Mo tips (No.1 and No.2), a commercial W tip, and a nipper-cut Mo wire. [Fig. 4b](#) shows the obtained I - V curves. All represents the Ohmic conductance. Since the nipper-cut Mo wire was coated by the oxide film (see [Fig. 1g](#)), its conductance was quite low ($R = 79 \Omega$, dotted line). However, the flame-etched Mo tips showed almost 20 times larger conductance ($R = 4.2$ and 4.3Ω , red and black solid lines), which are comparable to the commercial W tip probe ($R = 3.7 \Omega$, blue solid line).

Experimental evidence outlined in [Figs. 3 and 4](#) showed that the approximately 1 s flame etching at 2100 K performed twice, led to the production of a Mo tip shape with a radius of 50–100 nm; these Mo tips were confirmed to be available as probe tips through STM, FE, and conductance measurements. Since the flame etched Mo tip is prepared in air, any resultant contamination from the air is best excluded by UHV flushing, which also produces less noise data. Through the test measurements in [Figs. 3 and 4](#), we did not see any effects from the MoO₂ ball,

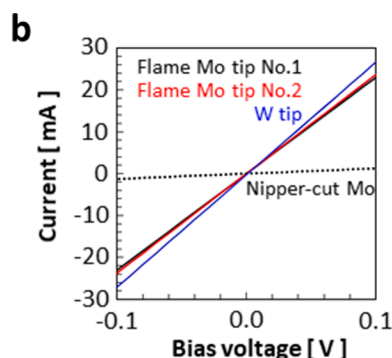
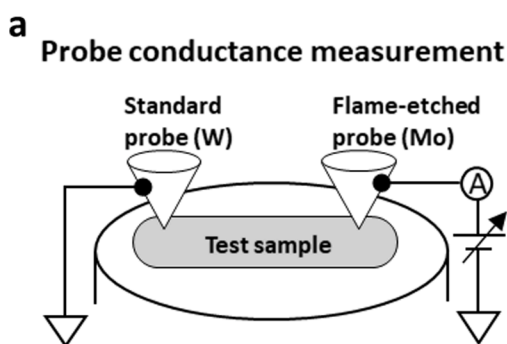


Fig. 4. Testing the flame-etched Mo tip probes. (a) Two-point contact conductance measurements. We used a standard W tip probe as the left-hand side probe and a Au film was used as a test sample. As the other tip probe, we used two flame-etched Mo tips (No.1 and No.2), a commercial W tip, and a nipper-cut Mo wire. (b) Conductance measurement results obtained from two flame-etched Mo tips: No.1 (black solid line) and No.2 (red solid line), a commercial W tip (blue solid line), and a nipper-cut Mo wire (dotted line).

which is located 0.2–0.5 mm far from the tip apex.

4. Conclusions

In summary, oxidative vaporization etching process in the LP and O₂ mixture gas flame with a temperature range of 1950–2300 K was employed to change a Mo wire edge to a tip shape in air. Especially, just by inserting a nipper-cut Mo wire edge within one second into the flame with a temperature of 2100 K (15 mm above the micro torch top) in air and repeated this motion twice, a sharp tip apex was reproducibly fabricated. The flame-etched Mo tips without any treatments in vacuum showed no crash of the tip and provided normal STM, field emission, and conductance results. Although a MoO₂ ball was always generated, we found that the Mo tip apex region was also simultaneously produced, which was occurred by the generation and immediate vaporization of MoO₃. No MoO₃ remained at the apex when we pulled out the Mo wire from the flame.

CRediT authorship contribution statement

Yuto Goto: Conceptualization, Methodology, Validation, Investigation, Writing - original draft. **Rie Suizu:** Validation, Investigation. **Yutaka Noguchi:** Investigation. **Toyo Kazu Yamada:** Conceptualization, Methodology, Validation, Investigation, Writing - review & editing, Supervision, Project administration, Funding acquisition.

Declaration of Competing Interest

The authors declare that they have no known competing financial interests or personal relationships that could have appeared to influence the work reported in this paper.

Acknowledgements

This work was supported by JSPS KAKENHI Grant Numbers 19H05789 and the Murata Science Foundation. We thank Mr. Satoru Sasaki for assistance of field emission spectroscopy measurements.

Appendix A. Supplementary data

Supplementary data to this article can be found online at <https://doi.org/10.1016/j.apsusc.2020.148642>.

References

- [1] T. Yamaguchi, E. Inami, Y. Goto, Y. Sakai, S. Sasaki, T. Ohno, T.K. Yamada, Fabrication of tungsten tip probes within 3 s by using flame etching, *Rev. Sci. Instrum.* 90 (2019), 063701.
- [2] A.I. Oliva, G.A. Romero, J.L. Pena, E. Anguiano, M. Aguilar, Electrochemical preparation of tungsten tips for a scanning tunneling microscope, *Rev. Sci. Instrum.* 67 (1996) 1917.
- [3] O.L. Guise, J.W. Ahner, M.-C. Jung, P.C. Goughnour, J.T. Jr, Yates, "Reproducible electrochemical etching of tungsten probe tips", *Nano Letters* 2 (2002) 191.
- [4] M. Kulakov, I. Luzinov, K.G. Kornev, Capillary and surface effects in the formation of nanosharp tungsten tips by electropolishing, *Langmuir* 25 (2009) 4462.
- [5] W.T. Chang, I.S. Hwang, M.T. Chang, C.Y. Lin, W.H. Hsu, J.L. Hou, Method of electrochemical etching of tungsten tips with controllable profiles, *Rev. Sci. Instrum.* 83 (2012), 083704.
- [6] Y. Khan, H. Al-Falih, Y. Zhang, T.K. Ng, B.S. Ooi, Two-step controllable electrochemical etching of tungsten scanning probe microscopy tips, *Rev. Sci. Instrum.* 83 (2012), 063708.
- [7] I. Ekvall, E. Wahlstrom, D. Claesson, H. Olin, E. Olsson, Preparation and characterization of electrochemically etched W tips for STM, *Meas. Sci. Technol.* 10 (1999) 11.
- [8] G.J. de Raad, P.M. Koenraad, J.H. Wolter, Use of the Schiller decapitation process for the manufacture of high quality tungsten scanning tunneling microscopy tips, *J. Vac. Sci. Tech. B* 17 (1999) 1946.
- [9] A.-S. Lucier, H. Mortensen, Y. Sun, P. Grütter, Determination of the atomic structure of scanning probe microscopy tungsten tips by field ion microscopy, *Phys. Rev. B* 72 (2005), 235420.
- [10] J. Onoda, S. Mizuno, H. Ago, STEM observation of tungsten tips sharpened by field-assisted oxygen etching, *Surf. Sci.* 604 (2010) 1094.
- [11] C. Vesa, R. Urban, J.L. Pitters, R.A. Wolkow, Robustness of tungsten single atom tips to thermal treatment and air exposure, *Appl. Surf. Sci.* 300 (2014) 16.
- [12] T.K. Yamada, M.M.J. Bischoff, T. Mizoguchi, H. van Kempen, Use of voltage pulses to detect spin-polarized tunneling, *Appl. Phys. Lett.* 82 (2003) 1437–1439.
- [13] A.N. Chaika, N.N. Orlova, V.N. Semenov, E.Y. Postnova, S.A. Krasnikov, M. G. Lazarev, S.V. Chekmazov, V.Y. Aristov, V.G. Glebovsky, S.I. Bozhko, I.V. Shvets, Fabrication of [001]-oriented tungsten tips for high resolution scanning tunneling microscopy, *Sci. Rep.* 4 (2014) 3742.
- [14] M.M.J. Bischoff, T.K. Yamada, C.M. Fang, R.A. de Groot, H. van Kempen, Local electronic structure of Fe(001) surfaces studied by scanning tunneling spectroscopy, *Phys. Rev. B* 68 (045422) (2003) 1–7.
- [15] L. Libiouille, Y. Houbion, J.M. Gilles, Very sharp platinum tips for scanning tunneling microscopy, *Rev. Sci. Instrum.* 66 (1995) 97.
- [16] J. Lindahl, T. Takanen, L. Montelius, Easy and reproducible method for making sharp tips of Pt/Ir, *J. Vac. Sci. Technol. B* 16 (1998) 3077.
- [17] A.H. Sørensen, U. Hvid, M.W. Mortensen, K.A. Mørch, Preparation of platinum / iridium scanning probe microscopy tips, *Rev. Sci. Instrum.* 70 (1999) 3059.
- [18] I.V. Borzenets, I. Yoon, M.W. Prior, B.R. Donald, R.D. Mooney, G. Finkelstein, Ultra-sharp metal and nanotube-based probes for applications in scanning microscopy and neural recording, *J. Appl. Phys.* 111 (2012), 074703.
- [19] B. Yang, E. Kazuma, Y. Yokota, Y. Kim, Fabrication of Sharp Gold Tips by Three-Electrode Electrochemical Etching with High Controllability and Reproducibility, *J. Phys. Chem. C* 122 (2018) 16950–16955.
- [20] R. Otero, A.L. Vazquez de Parga, J.M. Gallego, Electronic, structural and chemical effects of charge-transfer at organic / inorganic interfaces, *Surf. Sci. Rep.* 72 (2017) 105–145.
- [21] S. Schmaus, A. Bagrets, Y. Nahas, T.K. Yamada, A. Bork, F. Evers, W. Wulfhekel, Giant magnetoresistance through a single molecule, *Nat. Nanotechnol.* 6 (2011) 185–189.
- [22] G. Hörmandinger, Imaging of the Cu(111) surface state in scanning tunneling microscopy, *Phys. Rev. B* 49 (1994) 13897–13905.
- [23] J.A. Stroscio, D.T. Pierce, A. Davies, R.J. Celotta, M. Weinert, Tunneling Spectroscopy of bcc (001) Surface States, *Phys. Rev. Lett.* 75 (1995) 2960.
- [24] A. Bagrets, S. Schmaus, A. Jaafar, D. Kramczyński, T.K. Yamada, M. Alouani, W. Wulfhekel, F. Evers, Robust spin crossover and memristance across a single molecule, *Nat. Commun.* 3 (2012) 938.
- [25] T.K. Yamada, Y. Yamagishi, S. Nakashima, Y. Kitaoka, K. Nakamura, Role of π -d hybridization in 300-K organic-magnetic interface: metal-free phthalocyanine single molecules on bcc Fe(001)-whisker, *Phys. Rev. B* 94 (2016), 195437.
- [26] E.J. Heller, M.F. Crommie, C.P. Lutz, D.M. Eigler, Scattering and absorption of surface electron waves in quantum corrals, *Nature* 369 (1994) 464–466.
- [27] H.C. Manoharan, C.P. Lutz, D.M. Eigler, Quantum mirages formed by coherent projection of electronic structure, *Nature* 403 (2000) 512–515.

- [28] L. Venkataraman, J.E. Klare, C. Nuckolls, M.S. Hybertsen, M.L. Steigerwald, Dependence of single – molecule junction conductance on molecular conformation, *Nature* 442 (2006) 904–907.
- [29] S.Y. Quek, M. Kamenetska, M.L. Steigerwald, H.J. Choi, S.G. Louie, M.S. Hybertsen, J.B. Neaton, L. Venkataraman, Mechanically controlled binary conductance switching of a single – molecule junction, *Nat. Nanotechnol.* 4 (2009) 230–234.
- [30] Y. Kitaguchi, S. Habuka, H. Okuyama, S. Hatta, T. Arugam, T. Frederiksen, M. Paulsson, H. Ueba, Controlling single-molecule junction conductance by molecular interactions, *Sci. Rep.* 5 (2015) 11796.
- [31] T. Miyamachi, T. Schuh, T. Markl, C. Bresch, T. Balashov, A. Stohr, C. Karlewski, S. andre, M. Marthaler, M. Hoffmann, M. Geilhufe, S. Ostanin, W. Hergert, I. Mertig, G. Schon, A. Ernst, and W. Wulfhekel, Stabilizing the magnetic moment of single holmium atoms by symmetry, *Nature* 503, 242–246 (2013).
- [32] A.A. Khajetoorians, M. Steinbrecher, M. Ternes, M. Bouhassoune, M. dos Santos Dias, S. Lounis, J. Wiebe, R. Wiesendanger, Tailoring the chiral magnetic interaction between two individual atoms, *Nat. Commun.* 7 (2016) 10620.
- [33] M. Gobbi, M.A. Novak, E.D. Barco, Molecular spintronics, *J. Appl. Phys.* 125 (2019), 240401.
- [34] S.N. Kempkes, M.R. Slot, J.J. van der Broeke, P. Capiod, W.A. Benalcazar, D. Vanmaekelbergh, D. Bercioux, I. Swart, C.M. Smith, Robust zero-energy modes in an electronic higher-order topological insulator, *Nat. Mater.* 18 (2019) 1292–1297.
- [35] J. Su, M. Telychko, P. Hu, G. Macam, P. Mutombo, H. Zhang, Y. Bao, F. Cheng, Z. Q. Huang, Z. Qiu, S.J.R. Tan, H. Lin, P. Jelinek, F.C. Chuang, J. Wu, J. Lu, Atomically precise bottom-up synthesis of π -extended [5]triangulene, *Sci. Adv.* 5 (2019) eaav7717.
- [36] P. Willke, Y. Bae, K. Yang, J.L. Lado, A. Ferron, T. Choi, A. Ardavan, J. Fernandez-Rossier, A.J. Heinrich, C.P. Luts, Hyperfine interaction of individual atoms on a surface, *Science* 362 (2018) 336–339.
- [37] J. Friedlein, J. Harm, P. Lindner, L. Bargsten, M. Bazarnik, S. Kraus, R. Wiesendanger, A radio-frequency spin-polarized scanning tunneling microscope, *Rev. Sci. Instrum.* 90 (2019), 123705.
- [38] T. Kanagawa, R. Hobara, I. Matsuda, T. Tanikawa, A. Natori, S. Hasegawa, Anisotropy in Conductance of a Quasi-One-Dimensional Metallic Surface State Measured by a Square Micro-Four-Point Probe Method, *Phys. Rev. Lett.* 91 (2003), 036805.
- [39] T. Uchihashi, P. Mishra, M. Ando, T. Nakayama, Macroscopic Superconducting Current through a Silicon Surface Reconstruction with Indium Adatoms: Si(111)-($\sqrt{7} \times \sqrt{3}$)-In, *Phys. Rev. Lett.* 107 (2011), 207001.
- [40] M. Koch, F. Ample, C. Joachim, L. Grill, Voltage-dependent conductance of a single graphene nanoribbon, *Nat. Nanotechnol.* 7 (2012) 713–717.
- [41] S. Kawai, S. Saito, S. Osumi, S. Yamaguchi, A.S. Foster, P. Spijkier, E. Meyer, Atomically controlled substitutional boron-doping of graphene nanoribbons, *Nat. Commun.* 6 (2015) 8098.
- [42] T.K. Yamada, H. Fukuda, T. Fujiwara, P. Liu, K. Nakamura, S. Kasai, A.L. Vazquez de Parga, H. Tanaka, Energy Gap Opening by Crossing Drop Cast Single-Layer Graphene Nanoribbons, *Nanotechnology* 29 (2018), 315705.
- [43] E.W. Mueller, Das feldionenmikroskop, *Z. Phys.* 131 (1951) 136.
- [44] T.K. Yamada, T. Abe, N.M.K. Nazriq, T. Irisawa, Electron-bombarded $\langle 110 \rangle$ -oriented tungsten tips for stable tunneling electron emission, *Rev. Sci. Instrum.* 87 (2016), 033703.
- [45] R. Turan, D.D. Perovic, Mapping electrically active dopant profiles by field-emission scanning electron microscopy, *Appl. Phys. Lett.* 69 (1996) 1593.
- [46] T. Irisawa, T.K. Yamada, T. Mizoguchi, Spin polarization vectors of field emitted electrons from apexes of Fe-coated W tips, *New J. Phys.* 11 (2009), 113031.
- [47] G. Binnig, H. Rohrer, Scanning tunneling microscopy, *Surf. Sci.* 126 (1983) 236–244.
- [48] F.J. Giessibl, The qPlus sensor, a powerful core for the atomic force microscope, *Rev. Sci. Instrum.* 90 (2019), 011101.
- [49] D.H. Killeffer, A. Linz, Molybdenum Compounds: Their Chemistry and Technology, Interscience Publisher, New York, 1952.
- [50] P.E. Blackburn, M. Hoch, H.L. Johnston, The Vaporization of Molybdenum and Tungsten Oxides, *J. Phys. Chem.* 62 (1958) 769–773.
- [51] T. Ressler, J. Wienold, R.E. Jentoft, T. Neisius, Bulk Structural Investigation of the Reduction of MoO₃ with Propene and the Oxidation of MoO₂ with Oxygen, *Journal of Catalysis* 210 (2002) 67–83.
- [52] E.A. Weiss, G.K. Kaufman, J.K. Kriebel, Z. Li, R. Schalek, G.M. Whitesides, Si/SiO₂-Templated Formation of Ultraflat Metal Surfaces on Glass, Polymer, and Solder Supports: Their Use as Substrates for Self-Assembled Monolayers, *Langmuir* 23 (2007) 9686–9694.
- [53] D. Errandonea, Improving the understanding of the melting behaviour of Mo, Ta, and W at extreme pressures, *Physica B* 357 (2004) 356–364.
- [54] Molybdenum – Melting Point and Boiling Point, <https://www.nuclear-power.net/molybdenum-melting-point-boiling-point/>.
- [55] P. Carozzo, F. Tumino, A. Facibeni, M. Passoni, C.S. Casari, A. Li Bassi, Note: Fabrication and characterization of molybdenum tips for scanning tunneling microscopy and spectroscopy, *Rev. Sci. Instrum.* 86 (2015), 016112.
- [56] J.H. Junga, N.Y. Lee, J. Jang, M.H. Ohc, S. Ahn, Electron emission performance of nitrogen-doped hydrogen-free diamond-like carbon coating on Mo-Tip field emitter arrays, *J. Vac. Sci. Technol. B* 18 (2000) 933.
- [57] N. Zhu, J. Chen, Design, Fabrication and Characterization of Molybdenum Field Emitter Arrays (Mo-FEAs), *Micromachines* 8 (2017) 162.
- [58] R. Nemoto, P. Krueger, A.N.P. Hartini, T. Hosokai, M. Horie, S. Kera, T.K. Yamada, Well-Ordered Monolayer Growth of Crown-Ether Ring Molecules on Cu(111) in Ultra-High Vacuum: An STM, UPS, and DFT Study, *J. Phys. Chem. C* 123 (2019) 18939–18950.
- [59] E. Inami, M. Yamaguchi, R. Nemoto, H. Yorimitsu, P. Krueger, T.K. Yamada, Direct Imaging of Precursor Adcomplex States during Cryogenic-Temperature On-Surface Metalation: Scanning Tunneling Microscopy Study on Porphyrin Array with Fe Adsorption at 78.5 K, *J. Phys. Chem. C* 124 (2020) 3621–3631.
- [60] E. Inami, M. Yamaguchi, T. Yamaguchi, M. Shimasaki, T.K. Yamada, Controlled Deposition Number of Organic Molecules Using Quartz Crystal Microbalance Evaluated by Scanning Tunneling Microscopy Single-Molecule-Counting, *Anal. Chem.* 90 (2018) 8954–8959.
- [61] E. Inami, M. Shimasaki, H. Yorimitsu, T.K. Yamada, Room temperature stable film formation of π -conjugated organic molecules on 3d magnetic substrate, *Sci. Rep.* 8 (2018) 353.
- [62] I. Horcas, R. Fernandez, WSXM: A software for scanning probe microscopy and a tool for nanotechnology, *Rev. Sci. Instrum.* 78 (2007), 013705.
- [63] G. Aoki, T.K. Yamada, M. Arii, S. Kojima, T. Mizoguchi, Requirement of Ala residues at g position in heptad sequence of α -helix-forming peptide for formation of fibrous structure, *J. Biochemistry* 144 (2008) 15–19.
- [64] T. Yamada, J. Fujii, T. Mizoguchi, STM, STS, and Local Work Function Study of Cs/p-GaAs(110), *Surf. Sci.* 479 (2001) 33–42.
- [65] R. Hammer, A. Sander, S. Forster, M. Kiel, K. Meinel, W. Widdra, Surface reconstruction of Au(001): High-resolution real-space and reciprocal-space inspection, *Phys. Rev. B* 90 (2014), 035446.